RSC Advances

PAPER

View Article Online
View Journal | View Issue

Cite this: *RSC Adv.*, 2022, **12**, 24743

Novel Janus $MoSiGeN_4$ nanosheet: adsorption behaviour and sensing performance for NO and NO_2 gas molecules

Yixin Weng,[a] Xinguo Ma,[*a] Gang Yuan,[a] Hui Lv[*b] and Zhongyong Yuan[*c]

A novel Janus $MoSiGeN_4$ nanosheet is proposed for detecting poisonous gas molecules. Herein, the adsorption behaviour and sensing performance of both sides of the $MoSiGeN_4$ monolayer to NO and NO_2 gas molecules were investigated by first-principles calculations. Firstly, it is found that the $MoSiGeN_4$ monolayer exhibits structural stability and indirect gap semiconductor characteristics. The largest adsorption energy of NO_2 molecules on the $MoSiGeN_4$ monolayer is −0.24 eV, which is higher than the −0.13 eV for NO molecules. Of course, the physisorption between gas molecules and the $MoSiGeN_4$ monolayer appears with slight charge transfer. It is confirmed that NO molecules and NO_2 molecules act as electron donors and electron acceptors, respectively. Meanwhile, the generation of small band gaps and impurity levels in the electronic structures after gas adsorption is in favour of the enhancement of electronic conductivity. Furthermore, the longest recovery times of NO and NO_2 molecules are predicted to be 0.15 and 10.67 ns at room temperature, and the lateral diffusion at the surface requires crossing a large energy barrier. These findings provide indisputable evidence for further design and fabrication of highly sensitive gas sensors based on the $MoSiGeN_4$ monolayer.

Received 27th June 2022
Accepted 17th August 2022

DOI: 10.1039/d2ra03957e

rsc.li/rsc-advances

1. Introduction

Recently, an increasing number of environmental problems such as photochemical smog and acid rain caused by poisonous gas molecules have been gradually highlighted.[1–3] Efficiently detecting these gas molecules is significant to industry, agriculture, and public health.[4] Current gas sensors are mainly designed based on metal–oxide–semiconductor,[5] polymers,[6] nanowires,[7] nanobelts[8] and two-dimensional (2D) materials,[9–11] *etc.* Among them, 2D materials have become a research hotspot due to their superior flexibility, large specific surface area, excellent electronic properties, and available active sites.[12–14] After the discovery of graphene,[15] gas sensors based on 2D materials have made significant progress.[16–21] For instance, Zhao *et al.* studied the interaction between the MoS_2 monolayer and various gas molecules and fully exploited its potential applications in gas sensors.[20] Ai *et al.* investigated the charge transfer mechanism of the WTe_2 monolayer with gas adsorption and presented that it could be used as a superior gas sensing material.[21] However, existing materials are not commendably satisfied with the increasing application demands such as high sensitivity, good selectivity, perfect stability and appropriate recovery time.[22]

Lately, a new 2D material of $MoSi_2N_4$ monolayer has been fabricated by chemical vapor deposition[23] and exhibited potential applications for the detection of NO and NO_2 molecules, while the deficiency still exists.[24] In general, conventional strategies including doping, structural defects, and construction of heterojunctions can be used to enhance the performance of 2D materials.[25–27] Interestingly, Cui *et al.* successfully synthesized a new 2D Janus structure of MoSSe monolayer, which showed better sensing performance than MoS_2 monolayer.[28] It is not unique, Dou *et al.* found that the sensitivity of WTe_2 monolayer for CO, NO, and O_2 molecules is significantly improved by constructing the Janus structure.[29] Inspired by the above research about Janus structure,[30–32] we envisaged to further enhance the adsorption performance of the $MoSi_2N_4$ monolayer for NO and NO_2 molecules in this way. Excitingly, Yu *et al.* proposed a 2D Janus structure of $MoSiGeN_4$ monolayer by first-principles calculations, which indeed exhibited more excellent stability and semiconducting properties.[33] But so far, there is no report on the Janus $MoSiGeN_4$ monolayer used in designing gas sensors.

Could Janus $MoSiGeN_4$ monolayer be a high-performance gas sensor? It is understood that the presence of inherent dipole moments and electric field in the material caused by the mirror asymmetry of the Janus structure apparently change its

[a]*School of Science, Hubei University of Technology, Wuhan 430068, China. E-mail: maxg@hbut.edu.cn*

[b]*Hubei Engineering Technology Research Centre of Energy Photoelectric Device and System, Hubei University of Technology, Wuhan 430068, China. E-mail: lvhui@hbut.edu.cn*

[c]*Key Laboratory of Advanced Energy Materials Chemistry (Ministry of Education), College of Chemistry, Nankai University, Tianjin 300071, China. E-mail: zyyuan@nankai.edu.cn*

electronic properties.[34,35] Based on this idea, we explored the adsorption behaviour and sensing performance of the Janus $MoSiGeN_4$ monolayer for NO and NO_2 gas molecules using density functional theory (DFT). Firstly, the structural stability of the $MoSiGeN_4$ monolayer was proved by the calculation of phonon dispersion spectra, elastic constants, and cohesive energy, respectively. Then, considering the feasible adsorption sites and orientations of the $MoSiGeN_4$ monolayer, the most stable adsorption configurations for NO or NO_2 molecules were determined by comparing the adsorption energy. Meanwhile, to explain the adsorption sensitivity in-depth, the energy band structures, the density of states (DOSs), and the charge density difference of the $MoSiGeN_4$ monolayer with gas adsorption were calculated, respectively, and the corresponding electronic conductivity was assessed. Finally, the recovery time of gas desorption and the transition state of gas lateral diffusion on the $MoSiGeN_4$ monolayer were discussed. Our research results demonstrate that the $MoSiGeN_4$ monolayer possesses several advantages over the $MoSi_2N_4$ monolayer, such as better selectivity and enhanced sensitivity, which makes it more suitable for designing highly sensitive gas sensors.

2. Calculation methods and models

All DFT calculations were completed using the Perdew–Burke–Ernzerhof (PBE) exchange-correlation functional in the framework of generalized gradient approximation (GGA) implemented by the CASTEP code.[36,37] The ultrasoft pseudo-potentials (USPs) were employed to optimize the structures. Simultaneously, Tkatchenko-Scheffler (TS) scheme for a hybrid semi-empirical solution was used to describe the van der Waals (vdW) interaction between gas molecules and the substrate.[38] Besides, the reliability of the results was checked by Ortmann–Bechstedt–Schmidt (OBS) within the Perdew–Wang (PW91) functional.[39] The valence atomic configurations were taken as Mo: $4s^2 4p^6 4d^5 5s^1$, Ge: $4s^2 4p^2$, Si: $3s^2 3p^2$, and N: $2s^2 2p^3$, respectively. In the process of the geometric structure optimization, a *k*-mesh with Monkhorst–Pack form of $3 \times 3 \times 1$ and a cut-off energy of 420 eV were taken.[40] A convergence accuracy of 5×10^{-5} eV per atom was used to relax atomic positions by minimizing the force on each atom in the BFGS minimization scheme.[41] The convergence criterion was 0.1 eV $Å^{-1}$ for the maximal force on atoms. The maximum displacement was 0.005 Å, and the stress convergence was less than 0.2 Gpa. Furthermore, the transition states were calculated using the LST/QST method.[42] Note that the spin polarization on all atoms was considered when calculating the magnetic moments of the NO and NO_2 molecules.

The top view and side view of two isomers M1 and M2 of Janus $MoSiGeN_4$ monolayer were shown in Fig. 1(a and b). It can be seen that the Janus $MoSiGeN_4$ monolayer is constructed by replacing Si atoms with Ge atoms on the side of the $MoSi_2N_4$ monolayer. Namely, the MoN_2 layer is sandwiched by the Si–N layer and the Ge–N layer, which breaks the original mirror symmetry of the $MoSi_2N_4$ monolayer.[33] In the M1 configuration, the outermost N and Mo atoms are at an angle in the horizontal plane. And in the M2 configuration, the outermost N atoms are located directly above the Mo atoms. To avoid the interactions between adjacent gas molecules, a $3 \times 3 \times 1$ supercell was built for calculation, which contains 9 Mo atoms, 9 Ge atoms, 9 Si atoms, and 36 N atoms. In addition, a 20 Å vacuum layer was employed to prevent the periodic interactions between the neighbouring slabs.

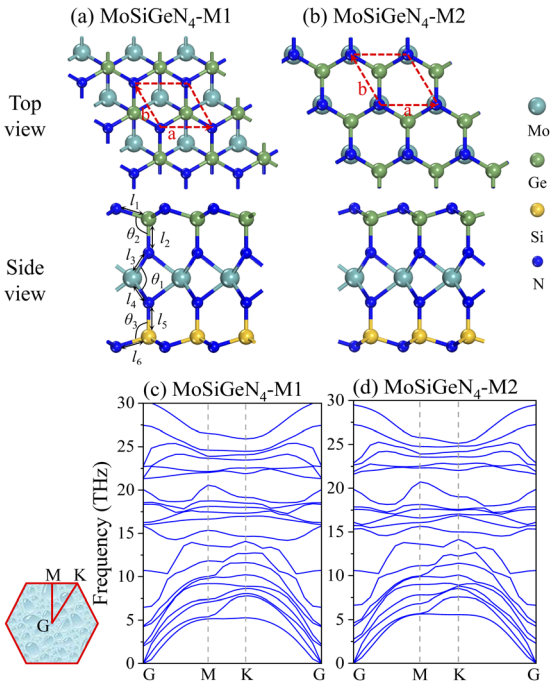

Fig. 1 The geometric structures of two kinds of isomers and the phonon dispersion spectra for the Janus $MoSiGeN_4$ monolayer. Here, the red dash line represents the rhombus primitive cell.

3. Results and discussion

3.1. Stability and electronic properties

The optimized lattice constants of two isomers M1 and M2 of Janus $MoSiGeN_4$ monolayer are 2.94 Å and 2.93 Å with PBE-TS, as shown in Table 1, which between those of $MoSi_2N_4$ (2.91 Å) and $MoGe_2N_4$ (3.02 Å).[43] Firstly, the dynamical stability of M1 and M2 are examined by analyzing the phonon dispersion spectra,[44] as shown in Fig. 1(c and d). Obviously, there are eighteen optical and three acoustical phonon branches can be observed, and the imaginary phonon modes are absent in the whole Brillouin zone, indicating that the two kinds of isomers are both dynamically stable. In addition, the mechanical stability of M1 and M2 was also checked by the elastic constants C_{ij}.[43] The Born criteria of the mechanical stability are $C_{11} > 0$, $C_{11}-C_{12} > 0$ for hexagonal symmetry. The calculated two independent elastic constants are $C_{11} = 496.474$ N m^{-1}, $C_{12} = 151.152$ N m^{-1} for M1, and $C_{11} = 493.394$ N m^{-1}, $C_{12} = 146.491$ N m^{-1} for M2. All results meet the above Born criteria, which demonstrates the mechanical stability of the $MoSiGeN_4$ monolayer.

To further quantitatively compare the structural stability of M1 and M2, the cohesive energy was calculated, which defines as the energy released by atoms in the process of transforming

Table 1 The calculated lattice constants, bond length, bond angle and cohesive energy of two kinds of isomers (M1 and M2) for the Janus $MoSiGeN_4$ monolayer

Model	Method	$a = b$ (Å)	l_1 (Å)	l_2 (Å)	l_3 (Å)	l_4 (Å)	l_5 (Å)	l_6 (Å)	θ_1 (°)	θ_2 (°)	θ_3 (°)	Cohesive energy (eV·per atom)
M1	PBE-TS	2.94	1.83	1.86	2.09	2.10	1.74	1.77	71.60	110.74	105.43	−7.35
	PW91-OBS	2.94	1.82	1.86	2.09	2.10	1.74	1.76	71.65	111.11	106.43	−7.33
M2	PBE-TS	2.93	1.82	1.87	2.09	2.10	1.75	1.77	72.09	111.88	105.64	−6.87
	PW91-OBS	2.93	1.82	1.87	2.09	2.10	1.75	1.76	72.17	111.74	106.29	−6.85

from free-state into bound-state: $E_{coh} = (E_{total} - \sum_i n_i E_i)/\sum_i n_i$, where E_{total} and n_i are the total energy and the amount of i-th atom in one unit cell, and E_i is the chemical potential of the i-th atom in its bulk element crystal.[33,45] Table 1 shows that the E_{coh} of M1 is −7.35 eV, which is higher than the −6.87 eV of M2. Generally, the higher the value of E_{coh}, the more stable the structure. Hence, M1 is more stable than M2, and M1 is chosen as the basis for the subsequent calculations. Meanwhile, Table 1 shows that the structural parameters of the two isomers are not significantly different, but two sides of the structure are asymmetric for a specific isomer. In the M1 configuration, the Ge–N bond lengths (l_1 = 1.83 Å, l_2 = 1.86 Å) are greater than Si–N bond lengths (l_6 = 1.77 Å, l_5 = 1.74 Å), and the angles of N–Ge–N (θ_2 = 110.74°) are also larger than the angles of N–Si–N (θ_3 = 105.43°).

The energy band structure along the G–M–K–G path and the partial DOSs (PDOSs) of the Janus $MoSiGeN_4$ monolayer were displayed in Fig. 2, respectively. It is found that the valence band maximum (VBM) and the conduction band minimum (CBM) are located at the G-point and K-point, respectively. The $MoSiGeN_4$ monolayer has an indirect band gap of 1.40 eV using GGA-PBE and 2.19 eV using HSE06.[46] Since the band gap of $MoSi_2N_4$ monolayer calculated by GGA-PBE (1.84 eV) is in good agreement with the experimental result.[23] To unify the calculation method and facilitate the comparison, the GGA-PBE method was also used in the electronic calculations of the $MoSiGeN_4$ monolayer. Besides, it can be found from PDOSs that the VBM and CBM are mainly contributed by Mo-d and N-p states. Thus, the adsorption behaviour and sensing performance of the gas molecules on the $MoSiGeN_4$ monolayer can be evaluated by the changes in the properties of Mo and N atoms in the following work.

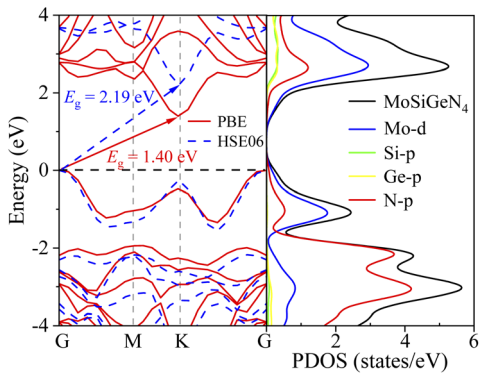

Fig. 2 Energy band structure of the Janus $MoSiGeN_4$ monolayer calculated by GGA-PBE and HSE06, and PDOSs of the $MoSiGeN_4$ monolayer calculated by GGA-PBE. Here, the Fermi level is set to zero and denoted by the black dash line.

3.2. Adsorption behaviour

The adsorption behaviour of the Janus $MoSiGeN_4$ monolayer can be characterized by adsorption energy, adsorption distance, and structural change. Here, to identify the optimal adsorption configurations for NO and NO_2 molecules, different adsorption sites and orientations were considered. Take the Ge–N side as an example; four possible adsorption configurations for NO or NO_2 molecules are shown in Fig. 3, namely: the top site of a N atom (Top-N), the top site of a Ge or Si atom (Top-Ge or Top-Si), the hollow site above the centre of the hexagon (Hollow) and the bridge site above the middle of a Ge–N or Si–N bond (Bridge).

The adsorption energy (E_a) of the Janus $MoSiGeN_4$ monolayer for gas molecules is expressed as follows

$$E_a = E_{total} - (E_{supercell} + E_{gas}) \quad (1)$$

where E_{total} represents the total energy of the adsorption system, $E_{supercell}$ represents the energy of the $MoSiGeN_4$ monolayer, and E_{gas} represents the energy of the free gas molecule.[47] Firstly, gas molecules were placed parallelly or perpendicularly on the different adsorption sites. Since the greater the value of E_a, the

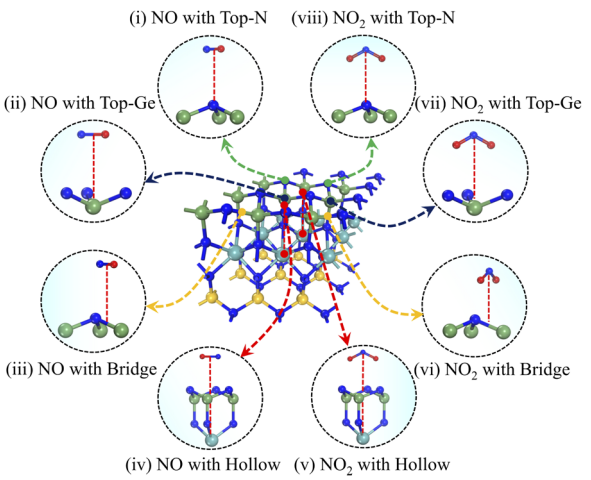

Fig. 3 The schematic diagrams of different adsorption configurations of NO or NO_2 molecules on the Janus $MoSiGeN_4$ monolayer.

Table 2 The calculated adsorption energy (E_a), adsorption distance (d) and recovery time (τ) of NO or NO_2 gas molecules on the Janus $MoSiGeN_4$ monolayer

Configuration		Ge–N side			Si–N side		
		E_a (eV)	d (Å)	τ (ns)	E_a (eV)	d (Å)	τ (ns)
NO	Hollow	−0.12	2.91	0.10	−0.13	2.80	0.15
	Top-Ge (Si)	−0.11	2.91	0.07	−0.10	2.80	0.05
	Top-N	−0.09	3.01	0.03	−0.07	2.81	0.01
	Bridge	−0.13	2.82	0.15	−0.11	2.80	0.07
NO_2	Hollow	−0.14	2.64	0.22	−0.20	2.81	2.27
	Top-Ge (Si)	−0.14	2.64	0.22	−0.17	2.81	0.71
	Top-N	−0.20	2.63	2.27	−0.22	2.80	4.92
	Bridge	−0.22	2.63	4.92	−0.24	2.79	10.67

stronger the adsorption interaction. By comparison, the gas molecules are more stable parallel to the surface. The parallel adsorption energies of NO molecules are between −0.07 and −0.13 eV, and that of NO_2 molecules are between −0.14 and −0.24 eV. It is acknowledged that a negative value of E_a indicates that the adsorption process is an exothermic reaction, which induces the adsorption system to be more stable. Then, we obtained the adsorption distance of all configurations, which is defined as the shortest distance between the bottom of gas molecule and the surface of substrate. In general, high adsorption energy corresponds to small adsorption distance, as shown in Table 2. In addition, we found that the adsorption energy of the $MoSiGeN_4$ monolayer on N_2, O_2 and H_2O molecules in the air is low, which indicates that the adsorption of these gases has little effect on the $MoSiGeN_4$ monolayer.

Fig. 4 presents the most favourable adsorption configurations of NO or NO_2 molecule on the two sides of the Janus $MoSiGeN_4$ monolayer. It is found that the NO molecule is above the Ge–N bond on the Ge–N side and the centre of the hexagon on the Si–N side, respectively, as shown in Fig. 4(a and b). The axis orientation of the NO molecule is nearly parallel to the surface of the $MoSiGeN_4$ monolayer, and the O atom is slightly downward. The adsorption energies are both −0.13 eV, and the corresponding adsorption distances are 2.82 and 2.80 Å, respectively. Fig. 4(c and d) show that the NO_2 molecule is located in parallel on the Ge–N bond or Si–N bond, respectively, and the O atoms are downward. The adsorption energies are −0.22 and −0.24 eV, and the adsorption distances are 2.63 and 2.79 Å, respectively. The results show that the adsorption interaction of the NO_2 molecule is stronger than that of the NO molecule. Besides, compared with the adsorption behaviour of NO_2 molecule on the $MoSi_2N_4$ monolayer (E_a = −0.11 eV, d = 2.75 Å),[24] Janus structure possesses some advantages.

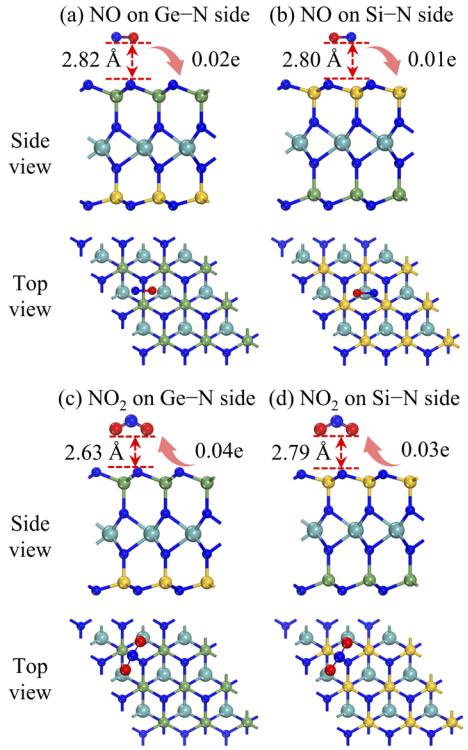

Fig. 4 Side and top views of the most stable adsorption configurations of the Janus $MoSiGeN_4$ monolayer adsorbed (a, b) NO or (c, d) NO_2 molecules. Here, the orientation and values of charge transfer are also denoted.

Due to the asymmetry of the Janus structure, the adsorption behaviour of the $MoSiGeN_4$ monolayer for NO or NO_2 molecules exhibit better selectivity than that of the $MoSi_2N_4$ monolayer. To be specific, the E_a for NO_2 molecule is always higher than that for NO molecule no matter which side of the Janus $MoSiGeN_4$ monolayer is adsorbed. Thus, it is inferred that its selectivity for NO_2 molecule is better than that for NO molecule. Meanwhile, the NO molecule has larger adsorption energy on the Ge–N side, but the NO_2 molecule has larger adsorption energy on the Si–N side, which indicates the selectivity of the Janus structure. Subsequently, the effects of NO or NO_2 adsorption on the substrate structure were evaluated. It can be found that the $MoSiGeN_4$ monolayer has a slight deformation around the adsorption sites, the bond length changed by about 0.1 Å, and the bond angle changed between 0.1° and 0.4°, as shown in Table 3. In summary, since the adsorption energy is small, the adsorption distance is large, and the structural deformation of the $MoSiGeN_4$ monolayer is not obvious, it is demonstrated that the interactions between the gas molecules and the substrate are weak, which can be characterized as physisorption.[24] Fortunately, the inherent magnetic properties of NO and NO_2

Table 3 The calculated bond length, bond angle, band gap and magnetic moment of the Janus $MoSiGeN_4$ monolayer after gas adsorption

Configuration	l_1 (Å)	l_2 (Å)	l_3 (Å)	l_4 (Å)	l_5 (Å)	l_6 (Å)	θ_1 (°)	θ_2 (°)	θ_3 (°)	E_g (eV)	M (μ_B)
NO on Ge–N side	1.81	1.86	2.09	2.10	1.74	1.77	71.48	111.14	105.84	0.49	1.11
NO on Si–N side	1.85	1.86	2.09	2.10	1.74	1.76	71.52	111.37	105.65	0.46	1.12
NO_2 on Ge–N side	1.82	1.86	2.09	2.10	1.74	1.77	71.41	111.14	105.84	0.47	1.13
NO_2 on Si–N side	1.85	1.86	2.09	2.10	1.74	1.77	71.47	111.46	105.79	0.20	1.11

molecules make them easier to be detected in the asymmetric Janus $MoSiGeN_4$ monolayer, exhibiting excellent sensing performance.

3.3. Sensing performance

To understand the sensing performance of the Janus $MoSiGeN_4$ monolayer, the energy band structures and PDOSs of the $MoSiGeN_4$ monolayer with NO or NO_2 adsorption were calculated, as shown in Fig. 5. It is found that some spin-down and spin-up impurity levels appear near the Fermi level in the energy band structures. Specifically, for NO molecule, after adsorption on the Ge–N side, two spin-up and one spin-down impurity levels are located at 0.08, 0.49 and 0.91 eV near the Fermi level. And after adsorption on the Si–N side, two spin-up and one spin-down impurity levels are located at 0.06, 0.44 and 0.86 eV. From the PDOSs, it is indicated that these new impurity levels are mainly derived from the N-p and O-p orbitals. For NO_2 molecules, a spin-down impurity level is located at 0.47 eV near the Fermi level after adsorption on the Ge–N side, and a spin-down impurity level is located at 0.21 eV after adsorption on the Si–N side. Likewise, these impurity levels are also mainly contributed by the N-p and O-p orbitals. The appearance of these impurity levels induced by the NO or NO_2 adsorption significantly changes the electronic properties of the $MoSiGeN_4$ monolayer. Compared with the pristine Janus $MoSiGeN_4$ monolayer (see Fig. 2), it can be found that the band gap of the $MoSiGeN_4$ monolayer with NO or NO_2 adsorption on the Ge–N side decreases by 0.91 and 0.93 eV, respectively, while those on the Si–N side decreases by 0.94 and 1.20 eV, respectively. There is an exponential relationship between the electronic conductivity and the band gap of a material:

$$\sigma \propto \exp\left(\frac{-E_g}{2kT}\right) \quad (2)$$

where σ, E_g, k ($= 8.62 \times 10^{-5}$ eV K^{-1}) and T represent the electronic conductivity, band gap of the material, Boltzmann constant, and thermodynamic temperature, respectively.[48] Based on the definition, it is inferred that the decrease of band gap means the increase of electronic conductivity, which improves the sensing performance of the $MoSiGeN_4$ monolayer. Therefore, NO or NO_2 molecules can be efficiently detected during the adsorption process, particularly for the NO_2 adsorption, which induces the most significant electronic conductivity variation.

Meanwhile, to verify the influence of gas adsorption on the Janus $MoSiGeN_4$ monolayer in-depth, we presented the DOSs of NO and NO_2 molecules before and after adsorption. The DOSs curves of NO and NO_2 molecules are flipped and shifted, which are induced by the charge transfer between the gas molecules and the $MoSiGeN_4$ monolayer, as shown in Fig. 6. For NO adsorption, the DOSs curves are flipped, but the relative displacement is small

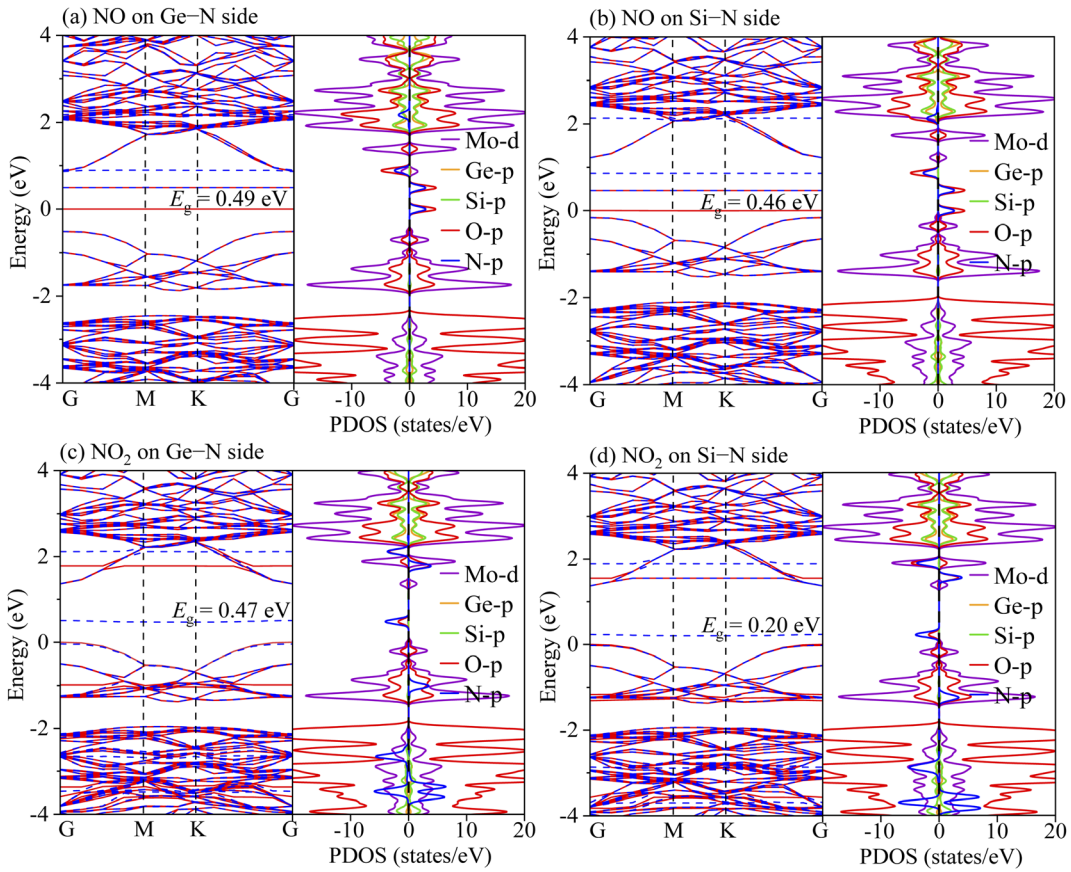

Fig. 5 Energy band structures and partial density of states (PDOSs) for (a, b) NO or (c, d) NO_2 molecules adsorption on the Janus $MoSiGeN_4$ monolayer. Here, the red solid lines and blue dash lines represent the energy band structures of spin-up and spin-down respectively.

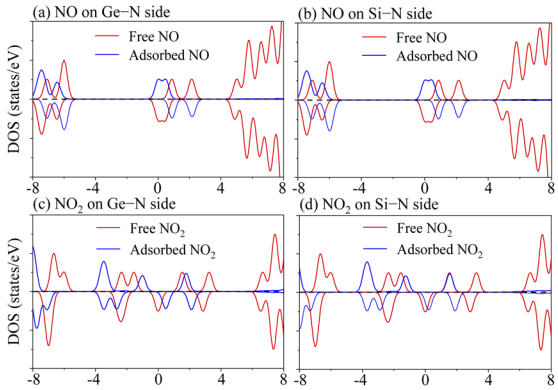

Fig. 6 Total density of states (TDOSs) of free NO or NO_2 molecules and partial density of states (PDOSs) of NO or NO_2 molecules in adsorption system.

near the Fermi level. For NO_2 adsorption, the DOSs curves are flipped and shifted apparently to the lower energy. Moreover, the pristine $MoSiGeN_4$ monolayer is nonmagnetic, but the NO or NO_2 adsorption introduces spin polarization in the system with a magnetic moment of approximately 1 μ_B, as shown in Table 3. It is concluded that the magnetic property of the $MoSiGeN_4$ monolayer is obviously caused by the gas adsorption, which reflects good sensing performance and makes these gas molecules easier to be detected.

More profoundly, we presented the charge density difference and the Mulliken populations to understand the sensitivity of the Janus $MoSiGeN_4$ monolayer for NO and NO_2 molecules. The charge density difference is defined as

$$\Delta\rho = \rho_{\text{total}} - (\rho_{\text{layer}} + \rho_{\text{gas}}) \quad (3)$$

where, ρ_{total}, ρ_{layer}, and ρ_{gas} represent the charge density of the $MoSiGeN_4$ monolayer with gas adsorption, the pristine $MoSiGeN_4$ monolayer, and the free gas molecules, respectively.[49] Fig. 7 shows the redistribution of the surface charge density. It can be seen that the change of charge distribution mainly occurs between the gas molecules and the $MoSiGeN_4$ monolayer. Subsequently, to quantitatively characterize the charge transfer, the Milliken populations were analyzed,[50] and presented in Fig. 4. Obviously, the NO molecule acts as an electron donor, losing 0.01e on the Si–N side and 0.02e on the Ge–N side. However, the NO_2 molecule acts as an electron acceptor, obtaining 0.03e on the Si–N side and 0.04e on the Ge–N side. Among them, the charge transfer value of 0.04e between the NO_2 molecule and the Ge–N side is the largest. There is a significant connection between the charge transfer and sensing performance; that is, the greater the charge transfer, the better the sensitivity of the substrate to the gas molecules. Therefore, the Janus $MoSiGeN_4$ monolayer exhibits better sensitivity to NO_2 molecules, which provides favourable conditions for its application as a gas sensor to detect NO_2 molecules.

3.4. Possibility as a gas sensor

Due to the physisorption of NO or NO_2 molecules, the electronic properties of the Janus $MoSiGeN_4$ monolayer change with the

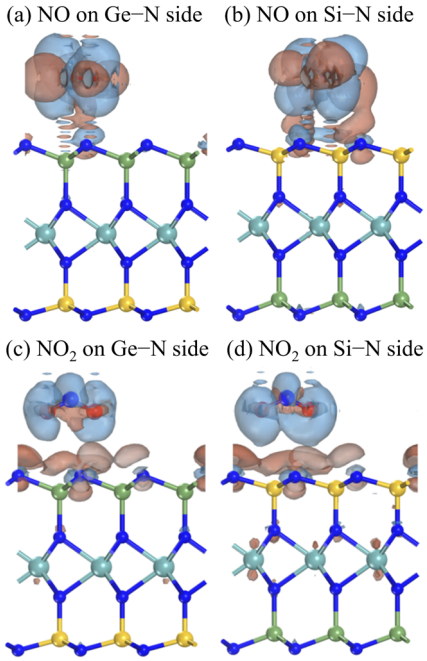

Fig. 7 Charge density differences of NO or NO_2 gas molecules adsorbed on the Janus $MoSiGeN_4$ monolayer. Here, the isovalue is set to 10^{-4} e Å^{-3}. The blue and red regions indicate charge accumulation and charge depletion, respectively.

slight charge transfer. Meanwhile, the decrease of band gap improves the electronic conductivity. Therefore, a resistive type gas sensor based on the $MoSiGeN_4$ monolayer can be designed to distinguish and detect NO and NO_2 molecules through the measurement of electronic signals affected by the resistance. Here, we discuss two important indicators of gas sensors, namely recovery time and sensitivity.

The recovery time is an essential parameter for gas sensors, which represents the time for gas molecules to desorb from the substrate. Gas sensors with good performance should possess the reusable characteristic, which requires a relatively short recovery time. According to the transition station theory, the functional relationship between the recovery time (τ) and the adsorption energy (E_a) can be expressed as

$$\tau = \nu_0^{-1} \exp\left(\frac{-E_a}{kT}\right) \quad (4)$$

where ν_0 ($=10^{12}$ s^{-1}), E_a, k and T represent the attempt frequency, adsorption energy, Boltzmann constant, and desorbing temperature, respectively.[24,51] Here, an ambient temperature of 300 K was taken to calculate the recovery time. It can be found from Table 2 that the recovery time for NO molecule is 0.15 ns, which is the shortest. For NO_2 molecule on the Si–N bond, the recovery time reaches 10.67 ns, which is closely related to the strong adsorption interaction between the NO_2 molecule and the $MoSiGeN_4$ monolayer. In general, a short recovery time is conducive to the efficiency of gas detection. However, in the practical applications, effectively reading the sensing signal needs a certain time, which requires the recovery time to be within a suitable range. According to the study of A.

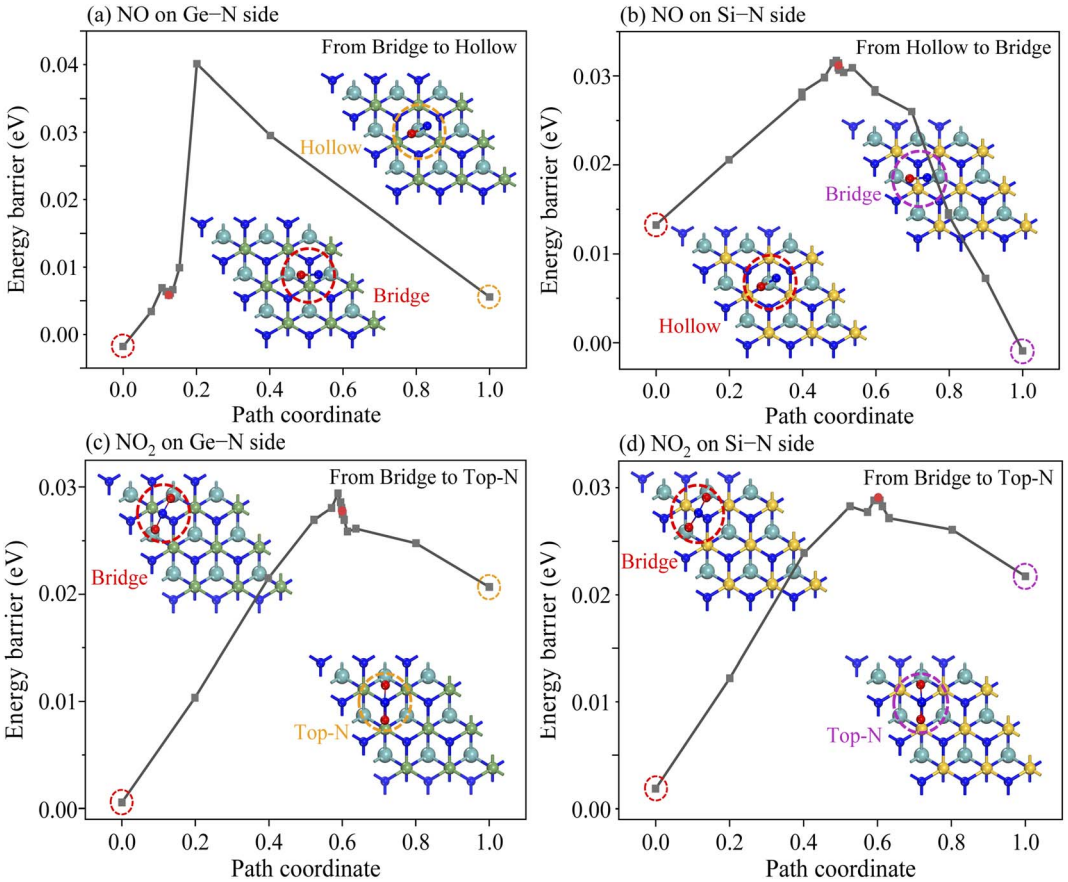

Fig. 8 Energy evolution profiles of NO and NO_2 molecules adsorbed on the Janus $MoSiGeN_4$ monolayer from the most stable site to the second stable site.

Bafekry,[24] the recovery times of the $MoSi_2N_4$ monolayer are 0.06 and 1.10 ns for NO and NO_2 molecule detection, respectively. It is illustrated that the recovery times of the $MoSiGeN_4$ monolayer are slightly longer. The results indicate that the $MoSiGeN_4$ monolayer has the feasibility to be used as promising NO and NO_2 gas sensors.

In addition to considering the gas desorption from the Janus $MoSiGeN_4$ monolayer, whether or not the gas molecules will diffuse laterally on the surface of the substrate is another crucial issue, since it is directly related to the accuracy of the gas sensors and the stability of sensing signal.[52,53] Based on this consideration, the most stable adsorption configuration and the second stable adsorption configuration of NO or NO_2 molecules on the $MoSiGeN_4$ monolayer were taken as the initial state and the final state, respectively. Fig. 8 shows the transition states in the diffusion processes of NO or NO_2 molecules on two sides of the Janus $MoSiGeN_4$ monolayer. On the Ge–N side, the energy barrier of NO_2 molecule diffused from the Bridge site to the Top-N site is about 0.27 eV, which is close to that on the Si–N side. Compared with the diffusion of NO molecule, the energy barriers of NO_2 molecule are significantly larger, which indicates that the NO_2 adsorption is more conducive to the stable transmission of sensing signals. This conclusion is consistent with the previous discussion about adsorption energy and charge transfer. Additionally, it is worth noting that the diffusion of the NO molecule on the two sides of the Janus $MoSiGeN_4$ monolayer is different, which may originate from the selectivity of the $MoSiGeN_4$ monolayer to the NO molecule. A large energy barrier provides a guarantee for the accuracy of the gas sensors and the stability of the sensing signal. Thus, the sensing signal of the NO_2 adsorption on the $MoSiGeN_4$ monolayer is reliable.

4. Conclusions

The adsorption behaviour and sensing performance of the Janus $MoSiGeN_4$ monolayer for NO and NO_2 molecules had been systematically investigated by first-principles calculations. It is found that the $MoSiGeN_4$ monolayer exhibits structural stability and indirect gap semiconductor characteristic. The adsorption strength of the NO_2 molecule on the Si–N side is stronger than that on the Ge–N side, while the NO molecule is opposite. Of course, both sides exhibit stronger adsorption interaction to the NO_2 molecule, which indicates that the $MoSiGeN_4$ monolayer has better selectivity to the NO_2 molecule. Besides, the NO or NO_2 adsorption can both induces the decrease of band gap and the emergence of impurity levels in the band structures, which significantly improves the electronic conductivity. The charge transfer of 0.03–0.04*e* between the NO_2 molecule and the substrate surface shows that the $MoSiGeN_4$

monolayer is sensitive to the NO_2 molecule. In addition, it is confirmed that the recovery time of the NO_2 desorption on the Si–N side of the $MoSiGeN_4$ monolayer is longer, and the lateral diffusion is not easy to happen at an ambient temperature. Thus, it is predicted that the sensing signal of the NO_2 molecule is possible to be detected on the $MoSiGeN_4$ monolayer. The above conclusions provide guidance and support for the practical application of the $MoSiGeN_4$ monolayer as gas sensors, especially as a NO_2 gas sensor.

Author contributions

The manuscript was written through contributions from all authors. All authors have given approval to the final version of the manuscript.

Conflicts of interest

The authors declare no competing financial interest.

Acknowledgements

This work was supported by the National "111 Research Centre" of Microelectronics and Integrated Circuits, the Outstanding Talent Foundation for Green Industry Leading Plan of HBUT (JCRC2021003), the Technology Cooperation Key Research and Development Program of Science and Technology Agency in Hubei Province (2021EHB018).

Notes and references

1 Z. Zhang, M. Haq, Z. Wen, Z. Ye and L. Zhu, *Appl. Surf. Sci.*, 2018, **434**, 891–897.
2 J. S. Kim, J. W. Yoon, Y. J. Hong, Y. C. Kang, F. Abdel-Hady, A. A. Wazzan and J. H. Lee, *Sens. Actuators, B*, 2016, **229**, 561–569.
3 M. R. Wu, W. Z. Li, C. Y. Tung, C. Y. Huang, Y. H. Chiang, P. L. Liu and R. H. Horng, *Sci. Rep.*, 2019, **9**, 7459–7467.
4 M. Kampa and E. Castanas, *Environ. Pollut.*, 2008, **151**, 362–367.
5 K. Wetchakun, T. Samerjai, N. Tamaekong, C. Liewhiran, C. Siriwong, V. Kruefu, A. Wisitsoraat, A. Tuantranont and S. Phanichphant, *Sens. Actuators, B*, 2011, **160**, 580–591.
6 B. Hua and G. Shi, *Sensors*, 2007, **7**, 267–307.
7 J. Kong, N. R. Franklin, C. Zhou, M. G. Chapline and H. Dai, *Science*, 2000, **287**, 622–625.
8 E. Comini, G. Faglia, G. Sberveglieri, Z. Pan and Z. L. Wang, *Appl. Phys. Lett.*, 2002, **81**, 1869–1871.
9 Y. Yong, X. Su, H. Cui, Q. Zhou, Y. Kuang and X. Li, *ACS Omega*, 2017, **2**, 8888–8895.
10 N. Hakimi Raad, N. Manavizadeh, I. Frank and E. Nadimi, *Appl. Surf. Sci.*, 2021, **565**, 150454–150460.
11 S. Thomas, V. Kumar, D. R. Roy and M. A. Zaeem, *ACS Appl. Nano Mater.*, 2020, **3**, 10073–10081.
12 J. Zhang, L. Liu, Y. Yang, B. Green and D. Zeng, *Phys. Chem. Chem. Phys.*, 2021, **23**, 15420–15439.
13 J. Zhao, X. Huang, Y. Yin, Y. Liao, H. Mo, Q. Qian, Y. Guo, X. Chen, Z. Zhang and M. Hua, *J. Phys. Chem. Lett.*, 2021, **12**, 5813–5820.
14 Y. Kim, K. C. Kwon, S. Kang, C. Kim, T. H. Kim, S. P. Hong, S. Y. Park, J. M. Suh, M. J. Choi, S. Han and H. W. Jang, *ACS Sens.*, 2019, **4**, 2395–2402.
15 K. S. Novoselov, A. K. Geim, S. V. Morozov, D. Jiang, Y. Zhang, S. V. Dubonos, I. V. Grigorieva and A. A. Firsov, *Science*, 2004, **306**, 666–669.
16 Q. He, S. Wu, Z. Yin and H. Zhang, *Chem. Sci.*, 2012, **3**, 1764–1772.
17 F. Schedin, A. K. Geim, S. V. Morozov, E. W. Hill, P. Blake, M. I. Katsnelson and K. S. Novoselov, *Nat. Mater.*, 2007, **6**, 652–655.
18 Z. W. Hao, M. M. Dong, R. Q. Zhang, C. K. Wang and X. X. Fu, *Phys. Chem. Chem. Phys.*, 2021, **23**, 11852–11862.
19 S. Yang, C. Jiang and S. H. Wei, *Appl. Phys. Rev.*, 2017, **4**, 021304–021337.
20 S. Zhao, J. Xue and W. Kang, *Chem. Phys. Lett.*, 2014, **595–596**, 35–42.
21 W. Ai, X. H. Hu, L. Pan, C. C. Chen, Y. F. Wang and X. D. Shen, *Acta Phys. Sin.*, 2019, **68**, 197101–197108.
22 W. Yuan and G. Shi, *J. Mater. Chem. A*, 2013, **1**, 10078–10091.
23 Y. L. Hong, Z. Liu, L. Wang, T. Zhou and W. Ren, *Science*, 2020, **369**, 670–674.
24 A. Bafekry, M. Faraji, M. M. Fadlallah, A. Abdolahzadeh Ziabari, A. Bagheri Khatibani, S. A. H. Feghhi, M. Ghergherehchi and D. Gogova, *Appl. Surf. Sci.*, 2021, **564**, 150326–150332.
25 W. Li, C. Ding, J. Li, Q. Ren, G. Bai and J. Xu, *Appl. Surf. Sci.*, 2020, **502**, 144140–144149.
26 C. Xiao, Z. Ma, R. Sa, Z. Cui, S. Gao, W. Du, X. Sun and Q. Li, *ACS Omega*, 2022, **7**, 8706–8716.
27 X. Song, J. Hu and H. Zeng, *J. Mater. Chem. C*, 2013, **1**, 2952–2969.
28 J. Cui, T. Xiao, T. Xin, S. C. Smith, D. Ying and L. Kou, *J. Mater. Chem. A*, 2019, **7**, 1099–1106.
29 H. Dou, B. Yang, X. Hu, C. Huo, X. Wang and C. Shi, *Comput. Theor. Chem.*, 2021, **1195**, 113089–113096.
30 Q. Wu, L. Cao, Y. S. Ang and L. K. Ang, *Nano Express*, 2020, **1**, 010042–010049.
31 D. Wang, T. Lan, J. Pan, Z. Liu and M. Rong, *Sens. Actuators, A*, 2020, **311**, 112049–112071.
32 D. Singh and R. Ahuja, *Nanomaterials*, 2020, **10**, 2554–2570.
33 Y. Yu, J. Zhou, Z. Guo and Z. Sun, *ACS Appl. Mater. Interfaces*, 2021, **13**, 28090–28097.
34 X. Tang and L. Kou, *Phys. Status Solidi B*, 2022, **259**, 2100562–2100569.
35 Z. Wu, L. Li, T. Liao, X. Chen, W. Jiang, W. Luo, J. Yang and Z. Sun, *Nano Today*, 2018, **22**, 62–82.
36 W. Kohn and L. J. Sham, *Phys. Rev.*, 1965, **140**, A1133–A1138.
37 M. D. Segall, P. J. D. Lindan, M. J. Probert, C. J. Pickard, P. J. Hasnip, S. J. Clark and M. C. Payne, *J. Phys.: Condens. Matter*, 2002, **14**, 2717–2744.
38 A. Tkatchenko and M. Scheffler, *Phys. Rev. Lett.*, 2009, **102**, 073005–073008.

39 F. Ortmann, F. Bechstedt and W. G. Schmidt, *Phys. Rev. B: Condens. Matter Mater. Phys.*, 2006, **73**, 205101–205110.
40 H. J. Monkhorst and J. D. Pack, *Phys. Rev. B: Solid State*, 1976, **13**, 5188–5192.
41 F. L. Hirshfeld, *Theor. Chim. Acta*, 1977, **44**, 129–138.
42 B. Y. Wang, Z. R. Li, N. X. Tan, Q. Yao and X. Y. Li, *J. Phys. Chem. A*, 2013, **117**, 3279–3291.
43 S. D. Guo, W. Q. Mu, Y. T. Zhu, R. Y. Han and W. C. Ren, *J. Mater. Chem. C*, 2021, **9**, 2464–2473.
44 Y. Yin, D. Li, Y. Hu, G. Ding, H. Zhou and G. Zhang, *Nanotechnology*, 2020, **31**, 315709–315741.
45 X. Zhang, Y. Cui, L. Sun, M. Li, J. Du and Y. Huang, *J. Mater. Chem. C*, 2019, **7**, 13203–13210.
46 M. Marsman, J. Paier, A. Stroppa and G. Kresse, *J. Phys.: Condens. Matter*, 2008, **20**, 064201–064210.
47 F. Li and C. Shi, *Appl. Surf. Sci.*, 2018, **434**, 294–306.
48 Y. Yong, H. Cui, Q. Zhou, X. Su, Y. Kuang and X. Li, *RSC Adv.*, 2017, **7**, 51027–51035.
49 B. Cho, M. G. Hahm, M. Choi, J. Yoon, A. R. Kim, Y. J. Lee, S. G. Park, J. D. Kwon, C. S. Kim, M. Song, Y. Jeong, K. S. Nam, S. Lee, T. J. Yoo, C. G. Kang, B. H. Lee, H. C. Ko, P. M. Ajayan and D. H. Kim, *Sci. Rep.*, 2015, **5**, 8052–8057.
50 G. D. Re, P. Otto and J. Ladik, *Isr. J. Chem.*, 2013, **19**, 265–271.
51 Y. Yong, X. Su, Q. Zhou, Y. Kuang and X. Li, *Sci. Rep.*, 2017, **7**, 17505–17516.
52 P. Hu, S. Wang and Y. Zhuo, *Sep. Purif. Technol.*, 2021, **275**, 119182–119190.
53 P. Hu, Q. Weng, D. Li, T. Lv, S. Wang and Y. Zhuo, *Chemosphere*, 2020, **257**, 127243–127256.